Carbohydrate Polymers 103 (2014) 70–80

Contents lists available at ScienceDirect

Carbohydrate Polymers

journal homepage: www.elsevier.com/locate/carbpol

Characterisation and drug release performance of biodegradable chitosan–graphene oxide nanocomposites

Richard Justin, Biqiong Chen*

Department of Materials Science and Engineering, University of Sheffield, Mappin Street, Sheffield S1 3JD, England

ARTICLE INFO

Article history:
Received 28 August 2013
Received in revised form 1 December 2013
Accepted 4 December 2013
Available online 12 December 2013

Keywords:
Chitosan
Graphene oxide
nanocomposite
transdermal drug delivery

ABSTRACT

Biodegradable chitosan–graphene oxide (GO) nanocomposites possess improved mechanical properties and drug delivery performance over chitosan and could prove to be a viable, controlled and pH-sensitive transdermal drug delivery system. Chitosan nanocomposites containing varying GO contents and drug loading ratios were investigated. The nanocomposite with 2 wt % GO provided the optimal combination of mechanical properties and drug-loading capacity. It offered a faster and a more substantial release of drug than chitosan as well as a slower biodegradation rate, owing to the abundant oxygenated functional groups, hydrophilicity and large specific surface area of GO sheets. The drug delivery profiles of the nanocomposite were dependent on the drug loading ratio, with 0.84:1 being the best ratio of drug to GO for a quick and high release of the loaded drug. The nanocomposite also demonstrated pH sensitivity of drug release, releasing 48% less drug in an acidic condition than in a neutral environment.

1. Introduction

Chitosan, the linear (1-4)-2-amino-2-deoxy-β-D-glucan, having a degree of acetylation close to 0.20, is currently isolated from marine chitin (Muzzarelli, 2012; Muzzarelli et al., 2012). It is both a biocompatible and biodegradable polymer, and has been noted for its haemostatic properties which assist in the formation of clots and thereby stop bleeding (Rao & Sharma, 1997; Kumar, Muzzarelli, Muzzarelli, Sashiwa, & Domb, 2004; Busilacchi, Gigante, Mattioli-Belmonte, Manzotti, & Muzzarelli, 2013). Chitosan has shown good potential for use in drug-eluding polymeric devices, having been used before as a diluent in polymer-coated oral tablets, which allow sustained delivery of various hydrophobic and hydrophilic drugs or site specific delivery to the colon without digestive degradation via pH sensitivity (Akbuğa, 1993; Hou, Miyazaki, Takada, & Komai, 1985; Sawayanagi, Nambu, & Nagai, 1982; Tozaki et al., 1997). Chitosan has been integrated with other drug delivery routes, most notably with gels (Knapczyk, 1993; Kristl, Šmid-Korbar, Štruc, Schara, & Rupprecht, 1993), microspheres (Akbuğa & Durmaz, 1994; Jameela & Jayakrishnan, 1995; Lorenzo-Lamosa, Remuñán-López, Vila-Jato, & Alonso, 1998), nanoparticles of chitosan (Bal, Ding, Kersten, Jiskoot, & Bouwstra, 2010; Bal, Slütter, Jiskoot, & Bouwstra, 2011) and films (Portero, Remuñán-López, & Vila-Jato, 1998; Xie, Xu, & Gao, 2005).

Graphene is an atomically thick sheet of sp^2 carbon atoms and is the building block for other carbon structures like nanotubes, fullerenes and graphite (Geim & Novoselov, 2007). Graphene is a much sought after material as it was found to have the highest tensile strength (130 GPa) and Young's modulus (1 TPa) of any natural substance, a theoretical surface area of 2,630 $m^2\ g^{-1}$, electron mobility of 10,000 $cm^2\ v^{-1}\ s^{-1}$ and a thermal conductivity value of 4,000 W mK (Chen et al., 2012; Geim & Novoselov, 2007; Lee, Wei, Kysar, & Hone, 2008; Novoselov et al., 2004; Stoller, Park, Zhu, An, & Ruoff, 2008). Previous work has combined graphene oxide (GO) nanosheets, created by the oxidation of graphene nanosheets, and chitosan together at low concentrations to create strong, biodegradable and biocompatible chitosan–GO nanocomposites (Han, Yan, Chen, & Li, 2011; Pan, Wu, Bao, & Li, 2011; Yang, Tu, Li, Shang, & Tao, 2010). However, these papers mainly focused on mechanical properties and there is a literature gap regarding the use of chitosan–GO nanocomposites for drug delivery and the effect that the integration of GO can have on biodegradation. As GO has ample phenol hydroxyl, epoxide and carboxylic functional groups to allow for better bonding to other molecules (Pan, Bao, & Li, 2011a, 2011b), a large surface area, excellent dispersibility within water and other aqueous mediums, low nanotoxicology (Wang et al., 2010; Zhang et al., 2011a,b) and is easy to manufacture (Liu, Robinson, Tabakman, Yang, & Dai, 2011), it is considered highly interesting in the biomedical field including drug delivery. When conjugated to GO, hydrophobic drugs have been shown to be dispersible in water solutions while maintaining their original potency (Liu, 2009; Sun et al., 2008a,b; Zhang, Xia, Zhao, Liu, & Zhang, 2010). An increase in gene therapeutic transport for graphene bonded drugs has also been noted (Bao et al., 2011).

Polymer coated GO nanosheets have also been used as therapeutic carriers as the coating can improve the biocompatibility of

* Corresponding author. Tel.: +44 0 114 222 5958; fax: +44 0 114 222 5943.
E-mail address: biqiong.chen@sheffield.ac.uk (B. Chen).

0144-8617/$ – see front matter © 2013 Elsevier Ltd. All rights reserved.
http://dx.doi.org/10.1016/j.carbpol.2013.12.012

GO. Chitosan coated GO was used to load and deliver hydrophobic and aromatic drugs, proving to be both biocompatible and highly effective in cancer cell reduction (Rana et al., 2011). Gene therapies were also investigated, with GO coated with poly(ethyleneimine) increasing the transfection efficiency of plasmid DNA and short interfering RNA in comparison to free therapeutics (Feng, Zhang, & Liu, 2011; Zhang et al., 2011a,a). Despite these benefits, only a limited number of papers have been published that use GO to improve the drug release profiles of polymers. Hydrogels of poly(vinyl alcohol) and GO have been analysed as possible drug delivery devices, but the drug itself was not bonded to the GO (Bai, Li, Wang, & Shi, 2010; Liu, Hu, Chen, & Chen, 2012). A nanocomposite film of poly (sebacic anhydride) and GO was also studied, but here again the GO was only utilized as the reinforcing filler (Gao et al., 2011).

This work aims to investigate the effects of GO on the drug release profiles of chitosan as well as its mechanical properties and biodegradation rate, and to achieve optimized chitosan–GO nanocomposites for potential applications in load-bearing drug delivery devices such as microneedle arrays for transdermal drug delivery. It will determine the concentration of GO that provides the optimum mechanical and drug delivery properties, while also investigating the effect that drug loading ratios have on the release rate of drugs. Fluorescein sodium (FL) was selected as the drug model, used to analyse the release rate improvement of therapeutics from nanocomposites, due to its dispersibility within aqueous mediums and distinct absorption peaks between 450 to 500 nm, as well as a molecular weight of 376 g mol^{-1}, similar in size to several important drugs such as the cancer drug cisplatin, the non-steroidal anti-inflammatory indomethacin, the beta blocker propranolol hydrochloride and the vasodilator timolol maleate.

2. Experimental Section

2.1. Materials

Chitosan powder (M_w = 100,000–300,000, Acros Organics, deacetylation degree ≥ 90% as determined by free amine groups) was used as purchased from Fisher Scientific. The following chemicals were reagent grade and used as purchased from Sigma Aldrich; acetic acid, sulphuric acid, hydrogen peroxide, potassium permanganate, sodium nitrate, fluorescein sodium, phosphate buffered saline (PBS), lysozyme and graphite powder (≤20 μm).

2.2. Preparation of GO

The method for making GO has been described before by others (Marcano et al., 2010). Briefly, graphite (3 g) was added to sulphuric acid (H_2SO_4) (69 ml) and sodium nitrate ($NaNO_3$) (1.5 g). The mixture was stirred vigorously for 30 min in an ice bath. Nine grams of potassium permanganate ($KMnO_4$) was added slowly and heated up to 35 °C and stirred for 12 h. Another 9 g of $KMnO_4$ was added to the mixture and stirred for 12 h before being poured over a mixture of ice (400 ml) and 30% hydrogen peroxide (H_2O_2) (3 ml). The solution was filtered through a 200 μm sieve. The graphite oxide suspension was centrifuged at 8000 rpm for 1 h in an Eppendorf Centrifuge 5804 with the supernatant being discarded. The graphite oxide was dispersed in fresh distilled water for a total of five cycles to remove residual chemicals from the production process. Graphite oxide was dried in a vacuum oven and stored in powder form in a desiccator. When required, graphite oxide was exfoliated in distilled water for 2 h by a Fisherbrand sonication bath (230 V, 50 Hz) and centrifuged at 8000 rpm for 30 min to remove larger than desired particles. The supernatant dispersion was collected for use in the nanocomposites. The concentration of the aqueous GO dispersion was determined by evaporating a solution of known quantity and determining the remaining dried mass.

2.3. Loading of drug onto GO

Fluorescein sodium powder was added to a 2 wt % solution of GO in water and stirred for 24 h. Unbound FL in the supernatant was removed from the solution through intense centrifugation at 9500 rpm for 1 h. This process was repeated to ensure the removal of all unbound FL. The GO–FL hybrid was then re-dispersed in distilled water by stirring for 1 h.

2.4. Preparation of chitosan–GO nanocomposites

Chitosan powder was added to a solution of 2 wt % acetic acid in distilled water and stirred for 24 h to prepare the chitosan solution. Then, the required concentration (0.25, 0.5, 1, 2 and 5 wt %) of nanoparticle filler was added to the chitosan solution and mixed for 12 h. The resultant dispersion was degassed in a sonication bath for 30 min. The dispersion was poured into a Teflon mould and allowed to air dry. Prior to testing, film was conditioned in an oven for 1 h at 50 °C. Drug-loaded GO was also used to produce nanocomposites of GO–FL and chitosan using GO–FL nanohybrids containing 2 wt % GO and various amounts of FL.

2.5. Structural characterization of GO and nanocomposites

UV-Visible spectroscopy was performed on dispersions of nanoparticles by a Perkin Elmer Lambda 900 spectrometer between 200–800 nm at a resolution of 1 nm. Fourier transform infra-red (FT-IR) spectroscopy of nanocomposite films and GO–FL powder was achieved through a Perkin Elmer Spectrum 100 with ATR at a resolution of 1 cm^{-1}. A Veeco Dimension 3100 atomic force microscope (AFM) with Olympus AC160TS probes was used in tapping mode at 0.5 Hz to analyse the thickness and dimensions of GO sheets laid on a mica substrate. Laser scattering (LS) particle sizing of particles from 0.1 to 900 μm was achieved through a Coulter LS130 using 3 one minute runs of nanoparticles in a dispersion of GO (0.4 mg ml^{-1}). X-ray diffraction (XRD) analysis of the crystal structure was achieved by using a Stoe Stadi P with $CuK_{\alpha 1}$ irradiation (0.154 nm wavelength) with an imaging plate detector. Transmission electron microscopy (TEM) analysis was achieved using a FEI Tecnai Biotwin using bright field imaging at an accelerating voltage of 80 kV. TEM samples were prepared using a Reichert–Jung Ultracut E microtome. Zeta potential was measured using a Brookhaven ZetaPALS, with solution concentrations of 1 mg ml^{-1} and 5 cycles of 10 runs per sample. A Horiba Fluoromax-4 with excitation source of 480–500 nm (max excitation shown to be 495 nm) and emission readings from 500–600 nm was used for photoluminescence spectroscopy (using solutions of 45.6 wt % loaded GO–FL at 1 mg ml^{-1}, GO at 0.545 mg ml^{-1} which contains the same quantity of GO as in the GO–FL solution, and unbound FL at 0.456 mg ml^{-1} which contains the same quantity of FL as in the GO–FL solution).

2.6. Tensile testing of nanocomposites

Tensile testing was performed on a Zwick Roell Z005 twin column tensometer using a 5 kN load cell and a 1 mm min^{-1} strain rate in accordance with ISO-527. Specimens (n = 10) were created using a punch of a dog-bone shape with the narrow test section between grips measuring 22 mm in length, 2.7 mm in width and 1 mm in thickness.

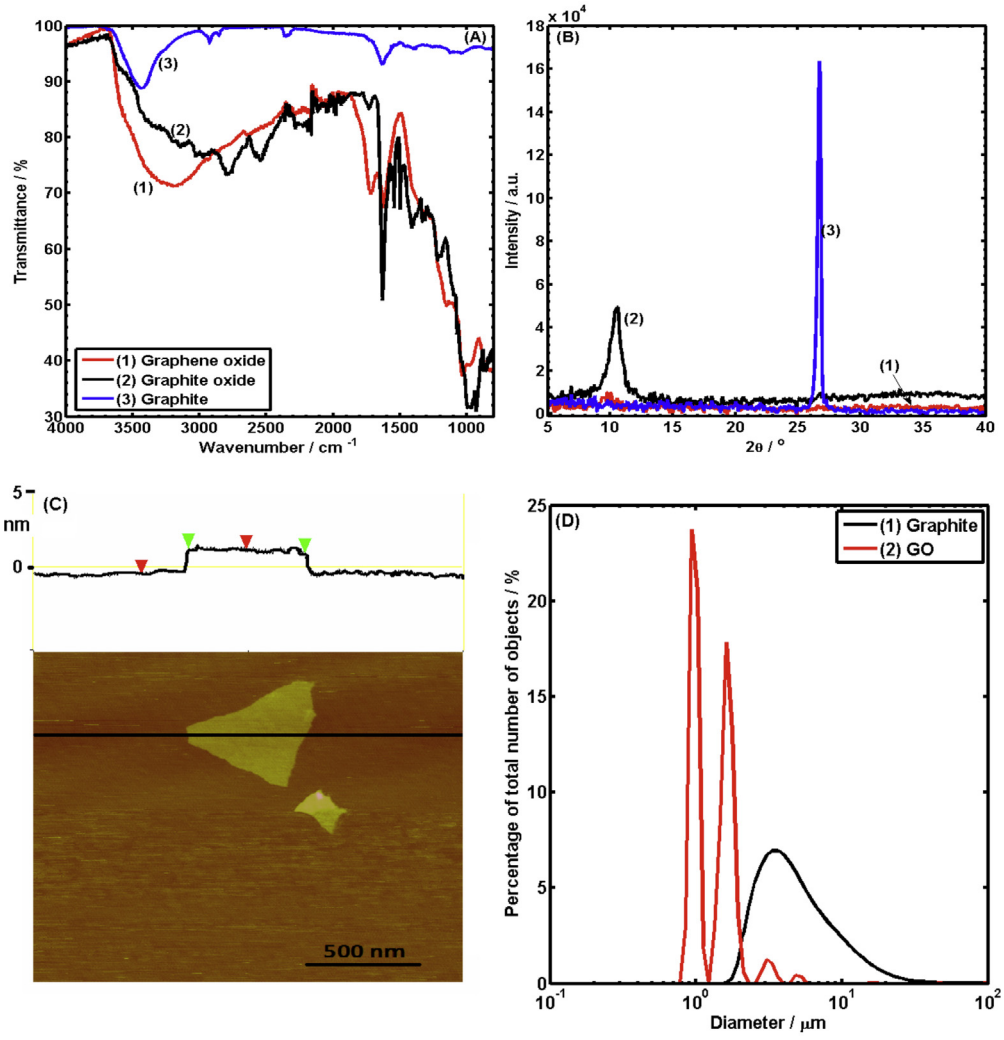

Figure 1. (A) FT-IR spectra and (B) XRD traces for GO, graphite oxide and graphite, (C) Atomic force microscopy image and height profiles of GO nanosheets and (D) laser scattering particle sizing profiles of GO nanosheets and graphite in an aqueous solution.

2.7. Drug release from nanocomposites

Nanocomposite specimens (n = 5) were placed in a PBS solution (30 ml) at 37 °C and gently agitated. A known quantity (2 ml) of solution from the container was removed after every time step, making sure to replace it with the same amount of fresh PBS solution. UV-Vis spectroscopy in a Perkin Elmer Lambda 900 determined the release rates of the drug from the nanocomposite in neutral (pH = 7.4) and acidic (pH = 2, 5.5 and 6.5) conditions. The quantity of FL was determined by comparing the absorbance peak at 450 nm of the test samples with solutions of free fluorescein of known concentration (from 0.001 to 1 mg ml^{-1}) in water, similar to the procedure used to measure the quantity of FL in solution during the loading of the drug onto the GO.

2.8. Biodegradation tests

Enzymatic biodegradation tests have been described elsewhere (Freier, Koh, Kazazian, & Shoichet, 2005; Tomihata & Ikada, 1997). Briefly, the polymer films were submersed in PBS solution (pH = 7) at 37 °C containing the enzyme lysozyme at a natural concentration as seen within the body, 1.5 μg ml^{-1} (Brouwer, van Leeuwen-Herberts, & de Ruit, 1984; Porstmann et al., 1989). Samples were maintained at 37 °C and were gently agitated. At regular intervals, each specimen was removed from the beaker, washed with distilled water, dried and the mass measured. The sample was placed into fresh PBS and lysozyme solution to maintain constant enzymatic activity. For each sample type, there were 5 specimens for mass analysis and two sacrificial specimens for characterization analysis.

2.9. Statistical analysis

Statistical analysis (standard deviation and 95% confidence intervals) were calculated using Matlab 2012a software.

3. Results and Discussion

3.1. Characterization of GO

GO, produced through exfoliation of graphite oxide created from a modified Hummers method, was characterized by FT-IR, XRD, AFM and LS to confirm the chemical bonds present, the interlayer spacing and the dimensions of the GO, respectively. Four main groups can be noted on the FT-IR spectra shown in Figure 1 (A): at 1043 cm^{-1} for C–O bonds; at 1628 cm^{-1} for C = C bonds; at 1727 cm^{-1} for C = O bonds and at 3400 cm^{-1} for O–H bonds from retained free water in the sample (K. Liu et al., 2011a,b; Marcano et al., 2010). The graphite curve has two main peaks, one at 3400 cm^{-1} (O–H bonds) from free water and a second at 1640 cm^{-1} (C = C bonds). The

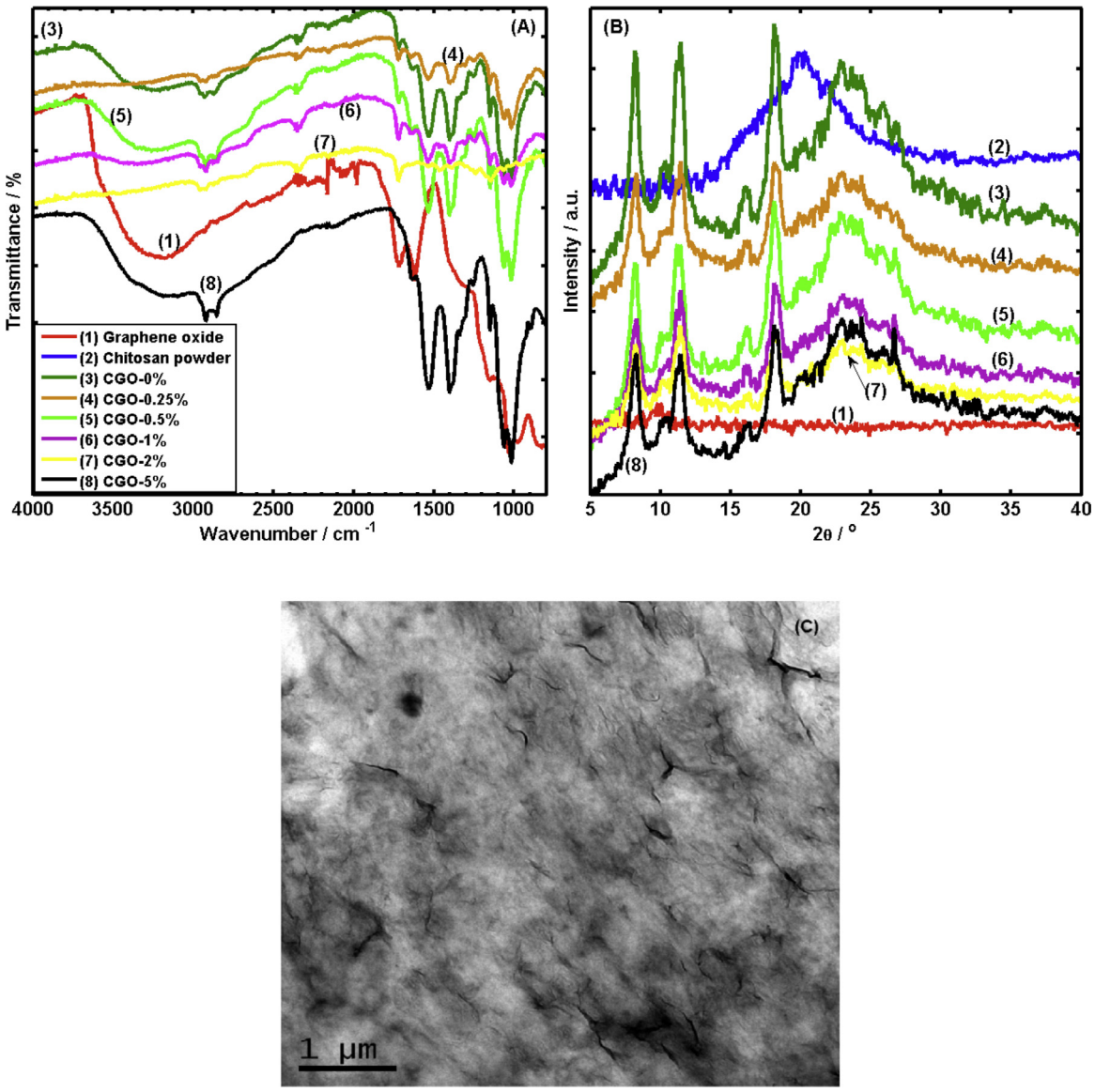

Figure 2. (A) FT-IR spectra, (B) XRD traces of chitosan nanocomposites containing 0–5 wt % GO, and (C) TEM micrograph of 2 wt % GO chitosan nanocomposite, showing a good dispersion of GO nanosheets.

process of oxidation introduces a peak at 1043 cm^{-1} (C–O bonds) and at 1727 cm^{-1} (C = O bonds) on the graphite oxide and GO curve.

Figure 1 (B) shows the XRD curves for graphite and graphite oxide, again demonstrating that the oxidation process was successful and changed the chemical structure of graphite. The (002) peak of graphite oxide is at $2\theta = 11^{o}$ corresponding to an interlayer spacing of 0.8 nm and the (002) peak of graphite is at $2\theta = 26^{o}$ corresponding to an interlayer spacing of 0.34 nm, similar to the published literature (Bissessur, Liu, White, & Scully, 2006; Guo et al., 2012). The low intensity of the peak at $2\theta = 10^{o}$ on the GO curve shows that the majority of nanosheets were exfoliated from graphite oxide to graphene oxide nanosheets (Fang, Wang, Lu, Yang, & Nutt, 2010; Kim, Abdala, & Macosko, 2010; Pan, Wu et al., 2011).

An AFM image of single layer thick GO nanosheets is shown in Figure 1 (C). The thickness of each layer is around 1.0 nm thick determined from several AFM images, showing the exfoliation of graphite oxide into single layer GO nanosheets (Pan, Wu et al., 2011; Yang et al., 2010a,b). The lateral size of GO nanosheets can be measured as approximately between 0.2 and 0.6 μm. This is a representative of a small sample size of the GO sheets. The LS size distribution of a greater sample size of GO sheets is shown in Figure 1 (D), showing that the majority of sheets range in size from 0.6 to 2 μm. The difference in size range between the AFM and LS values can be attributed to the fact that LS analysis measures the hydrodynamic diameter of GO particles and that it assumes these particles are spherical in shape. Graphite powder measured in size between 1 and 20 μm, showing that the oxidation and dispersion processes have successfully led to the production of smaller GO.

3.2. Characterization of nanocomposites

Chitosan nanocomposites of 0.25, 0.5, 1, 2, 5 wt % GO were created by dispersing known quantities of GO in chitosan solution and air drying. The nanocomposites will be designated as CGO–0%, CGO–0.25%, CGO–0.5%, CGO–1%, CGO–2%, CGO–5% for 0 (pristine chitosan), 0.25, 0.5, 1, 2 and 5 wt % nanocomposites, respectively. Characterization of the nanocomposites will allow for an analysis of the interfacial interactions, the GO dispersion and the crystallinity of the nanocomposites. An FT-IR analysis of chitosan nanocomposites containing 0–5 wt % GO is shown in Figure 2 (A). Prominent

peaks are similar to Figure 1 (A), showing strong C = C (1620 cm^{-1}), C = O (1720 cm^{-1}) and O–H bonds (3300–3400 cm^{-1}). An additional range of peaks can be seen at 2400–3200 cm^{-1}, which are N–H bonds from ammonium ions created by the deacetylation process, and at 1530–1540 cm^{-1}, which are amino groups from the chitosan (Lorenzo-Lamosa et al., 1998). At 1400 cm^{-1} C–OH bonds can be seen, and at 1000–1100 cm^{-1} C–O bonds can be seen (Han et al., 2011). The C–O bonds (from 1018 to 1012 cm^{-1} and from 1088 to 1084 cm^{-1} for pristine chitosan and the nanocomposites, respectively) and the amino group (from 1539 to 1531 cm^{-1} for pristine chitosan and the nanocomposites, respectively) have shifted significantly, indicating a strong hydrogen bonding between these two groups and the functional groups in GO (Han et al., 2011; Yang et al., 2010a,b).

An XRD analysis of the nanocomposites containing chitosan and GO is shown in Figure 2 (B). An amorphous structure for the chitosan powder can be identified as the broad peak at 20° (Rana et al., 2011). Diffraction peaks for all nanocomposites can be seen at 8, 11, 16, 18 and 23°, in keeping with the literature (Pan, Wu et al., 2011; Yang et al., 2010a,b). Peaks at 8, 11 and 18° are the result of a crystalline structure in chitosan while 16° and 23° are due to an amorphous structure in chitosan film (Yang et al., 2010a,b). Assuming no peaks for GO were present in the nanocomposite due to their low content and the strong interaction between GO and chitosan, which may lead to nearly full exfoliation (Yang et al., 2010a,b), the crystallinity percentage, χ_c, of nanocomposites can be determined from analyzing the diffraction peaks of chitosan, as shown in Eq. 1 (Galvan-Sanchez, Urena-Nunez, Flores-Llamas, & Lopez-Castanares, 1999; Nunes, Mahendrasingam, & Suryanarayanan, 2005). The TEM micrograph in Figure 2 (C) shows a good dispersion of GO nanosheets (shown as the black thin lines within the matrix, in accordance with the literature [e.g. Layek, Samanta, & Nandi, 2012; An & Jeong, 2013]) within the 2 wt % GO chitosan nanocomposite, the majority of which are exfoliated, confirming the validity of the assumption.

$$\chi_C = \frac{I_C}{I_C + I_A} \quad (1)$$

where I_c is the peak area of the crystalline region and I_a is the peak area of the amorphous region. The crystallinity values of chitosan nanocomposites are 30.5, 32.0, 23.3, 25.4, 27.3 and 21.5% for CGO–0%, CGO–0.25%, CGO–0.5%, CGO–1%, CGO–2%, CGO–5%, respectively. Solution casting has created crystalline regions within the chitosan film, which differentiates from the amorphous chitosan powder. The presence of 0.25 wt % GO slightly increased the crystallinity, owing to its nucleation effect (Chaudhry & Mittal, 2013). However, nanocomposites of higher GO contents have lower crystallinity than pristine chitosan films. Presumably, GO reduces the crystal growth by hindering the mobility of the chitosan chains, which outweighs the nucleation effect (Chaudhry & Mittal, 2013). The lowest crystallinity was measured for the sample CGO–5%.

3.3. Mechanical properties of nanocomposites

The nanocomposites can use GO as a structural reinforcement to improve mechanical properties as well as a drug carrier. Mechanical testing will allow for a determination of the optimum GO concentration to be used for the nanocomposite-based transdermal drug delivery devices which will require mechanical strength during application, such as microneedle arrays. The representative tensile stress–strain curves for chitosan and GO nanocomposites of CGO–0%, CGO–0.25%, CGO–0.5%, CGO–1%, CGO–2%, CGO–5% are shown in Figure 3.

The behaviour of the nanocomposites under strain varies depending on their GO content. Pristine chitosan samples undergo elastic deformation, yielding and necking without strain hardening.

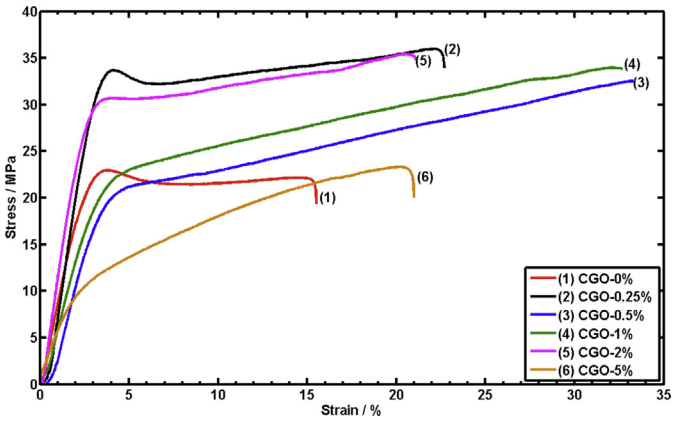

Figure 3. Tensile stress versus strain curves for chitosan nanocomposites containing 0–5 wt % GO.

CGO–0.25% (curve 2) and CGO–2% (curve 5) strain soften and then proceed to work hardening before failing. CGO–0.5%, CGO–1% and CGO–5% do not strain soften after yielding but proceed straight to work hardening before failing. The introduction of GO increases the ductility and ability of the samples to work harden when compared to the pristine chitosan sample.

The mechanical properties are summarized in Table 1. The pristine chitosan film fails at an average strain of 14.5%. The samples containing 0.25–5 wt % GO fail between 17.7 and 35.1% strain, demonstrating substantial increases in ductility of chitosan which are attributable to the orientation and delamination of graphene sheets under tension (Dasari, Yu, & Mai, 2007). CGO–0.25% and CGO–2% have the highest Young's modulus value of the sample range, with average Young's modulus values of 1.23 GPa and 1.30 GPa, respectively. GO has a higher Young's modulus than chitosan, 207 GPa versus 1 GPa (Suk, Piner, An, & Ruoff, 2010), and a high aspect ratio, a large specific surface area and abundant functional groups, thus acting as an effective reinforcement filler in these two cases. In contrast, CGO–0.5% and CGO–1% present lower modulus values. Both the effective volume fraction of GO and the effect of GO on polymer crystallinity affect the Young's modulus of the final nanocomposite (Chen & Evans, 2006). The former takes into account the contribution from the interfacial region and is therefore dependent on both the GO content and the dispersion degree of GO (Chen & Evans, 2006). Lower GO contents, e.g. 0.25 wt %, are expected to lead to better dispersion and therefore more efficient reinforcements. In comparison, the lower moduli exhibited by CGO–0.5% and CGO–1% nanocomposites can be attributable to their lower crystallinities. CGO–5% shows the lowest modulus, presumably due to the presence of defects and aggregates in addition to the low crystallinity, which is further discussed below. With the exception of CGO–5%, the addition of GO increased the ultimate tensile strength. CGO–0.25% and CGO-2% present the highest tensile strength among the materials tested, with increases of 43% and 37% compared to the value of their polymer counterpart. The strong bonding between GO and chitosan has allowed for an efficient transfer of stress from the chitosan to the GO nanosheets. Similar increases are expected for flexural modulus and flexural strength for the nanocomposites with small additions of GO (Tang et al., 2013).

An analysis of the fracture surface of tensile specimens (Figure S1, Supplemental Information) shows that as the GO content increases, the appearance of the fracture plane changes from smooth to pitted due to the layered structure of GO. Furthermore, the images for the nanocomposites containing 0–2 wt % GO show a uniform morphology throughout the fracture surface, while voids

Table 1
Tensile properties of chitosan–GO nanocomposites.

GO content (wt %)	Young's modulus (GPa)	Ultimate tensile strength (MPa)	Elongation at break (%)
0	1.00 ± 0.10	24.2 ± 1.4	14.5 ± 2.7
0.25	1.23 ± 0.12	34.5 ± 1.4	19.0 ± 2.2
0.5	0.86 ± 0.08	30.4 ± 1.8	25.9 ± 4.2
1	0.93 ± 0.13	32.4 ± 1.2	35.1 ± 2.6
2	1.30 ± 0.14	33.2 ± 2.2	17.7 ± 2.6
5	0.46 ± 0.11	21.9 ± 1.1	22.4 ± 3.3

and aggregations can be seen in the image for the sample with 5 wt % GO which may explain its inferior mechanical properties.

It is noteworthy that tensile test results were replicated by the creation and subsequent tensile testing of a new batch of nanocomposite samples and that the same mechanical behaviour was obtained for the second batch. Based on the above mechanical results, the two nanocomposites that possess the best mechanical properties are CGO–0.25% and CGO–2%. As a higher concentration of GO allows for a higher quantity of drug to be loaded onto GO than would be achievable with a lower concentration, the optimum nanofiller concentration for load-bearing drug delivery devices such as microneedle arrays is considered to be 2 wt %, and therefore it is used for subsequent drug delivery and biodegradation tests.

3.4. Characterization of FL-loaded GO hybrids

Drug coated GO was created through a simple mixing procedure and the removal of excess drug. The quantity of FL bonded to GO was determined by UV-Vis spectroscopy analysis by measuring the absorbance percentage of the characteristic peak (450 nm) of FL (Figure 4, inset). To calculate the drug loading ratio (FL:GO), the amount of unbound FL present in the supernatant prior to and after adsorbing onto GO was measured against the spectra of standard FL solutions with a known concentration. Drug loading ratio was calculated by:

$$Drug\ loading = \frac{Original - unbound\ FL\,(mg)}{Quantity\ of\ GO\,(mg)} \quad (2)$$

The drug loading ratio of FL to GO is dependent on the original concentration of the drug in the solution within the experiment time frame of 24 h. Figure 4 shows the increase in drug loading ratio when the original concentration of FL is varied from 0.1 mg ml^{-1} to 50 mg ml^{-1}, allowing for the selection of initial concentrations to make GO–FL powders with defined loading ratios. Initial concentrations of FL of 2.5 mg ml^{-1}, 12.5 mg ml^{-1} and 49 mg ml^{-1} were used to create nanohybrids with the loading ratios (FL:GO) of 0.28:1 (21.9 wt %), 0.84:1 (45.6 wt %) and 1.4:1 (58.3 wt %), respectively.

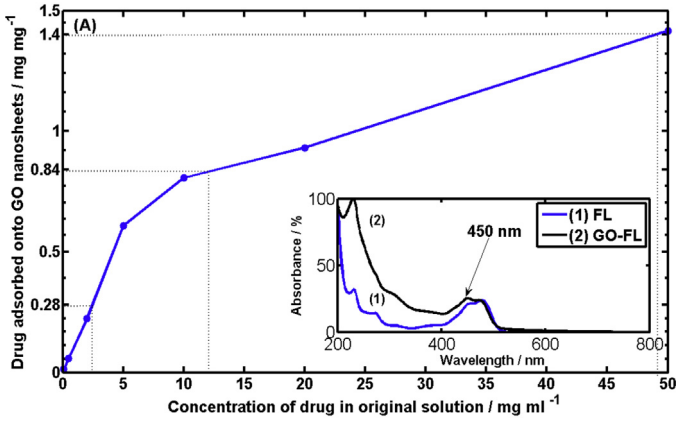

Figure 4. Drug loading chart of fluorescein sodium onto GO nanosheets as a function of initial FL concentration after 24 h of bonding. Inset: UV-Vis spectra of FL in water solution.

The successful bonding of FL onto GO surface can be confirmed by UV-Vis, FT-IR, photoluminescence spectroscopy and AFM. Figure 5 (A) shows the UV-Vis spectra of GO at the concentration of 0.4 mg ml^{-1} to allow for an analysis of absorption peaks. The peak at 230–235 nm can be attributed to $\pi \rightarrow \pi^*$ conjugations of C = C bonds and the peak at 300 nm is $n \rightarrow \pi^*$ conjugations of C = O bonds (Marcano et al., 2010). A comparison of unbound FL, FL–GO hybrid and GO nanosheets in Figure 5 (A) shows that the characteristic peaks of FL at 450 and 480 nm are present with a shift to 445 and 475 nm on the FL–GO hybrid curve, while a shoulder peak at 270–275 nm of the FL curve has been transposed onto the GO–FL curve but is not present on the GO curve.

FT-IR analysis of GO–FL and FL powders are shown in Figure 5 (B). In this figure, peaks characteristic of GO can be seen (C = O at 1720 cm^{-1}, C = C bonds at 1600 cm^{-1} and C–O bonds at 1000–1100 cm^{-1}) for the 45.6 wt % FL loaded GO–FL nanohybrid. Peaks characteristic of FL can be seen on the GO–FL curve below 1600 cm^{-1} and there is a shift in wavenumber on peaks (from 1738 for FL to 1726 cm^{-1} for GO–FL, from 1572 for FL to 1530 cm^{-1} for GO–FL, and from 1088 for FL to 1066 cm^{-1} for GO–FL) which can be attributed to both physical adsorption of the drug onto the surface and an overlapping of FL peaks with GO peaks. The bonding between GO and FL includes electrostatic forces and hydrogen bonding, as reported in the literature (Sari, 2013).

Photoluminescence spectra are shown in Figure 5 (C), showing the quenching effect of GO on GO–FL in comparison to free FL. The solutions of unbound FL and pristine GO were of a concentration equal to the quantity of FL or GO on the GO–FL in the 45.6 wt % FL loaded GO–FL nanohybrid solution. GO–FL has a photoluminescent property courtesy of the FL, as can be seen by comparing to the GO, again suggesting successful bonding of FL onto GO. An AFM image of a single GO–FL sheet from the 0.84:1 solution is shown in Figure 5 (D). It shows a sheet of an approximate thickness of 8.7 nm. The increase in thickness from 1 nm for GO is due to the coating of FL on the surface, which can be seen to be rough and uneven across the surface, emphasized by the AFM-3D image in Figure S2 (Supplemental Information). Zeta potential readings were taken before and after the synthesis of the 0.84:1 ratio solution, with values of -53.58 (± 0.96) mV for GO and -54.54 (± 0.76) mV for GO–FL, implying both have good stability in aqueous solutions and that the negative electrical charge of GO is only slightly increased by the addition of FL.

3.5. Drug release from nanocomposite

The release rate and quantity released are important to determine for a drug delivery mechanism, which can be analyzed using UV-Vis spectroscopy. Figure S3 (Supplemental Information) shows a comparison of free FL, GO–FL encapsulated nanocomposites and the FL released during testing. The characteristic peaks of the FL at 450 nm and 480 nm in the free FL have shifted back from 445 nm and 475 nm for the GO–FL after being released from the nanocomposite into the PBS medium, which indicates a possible unbinding of FL from GO after release and is coincident with

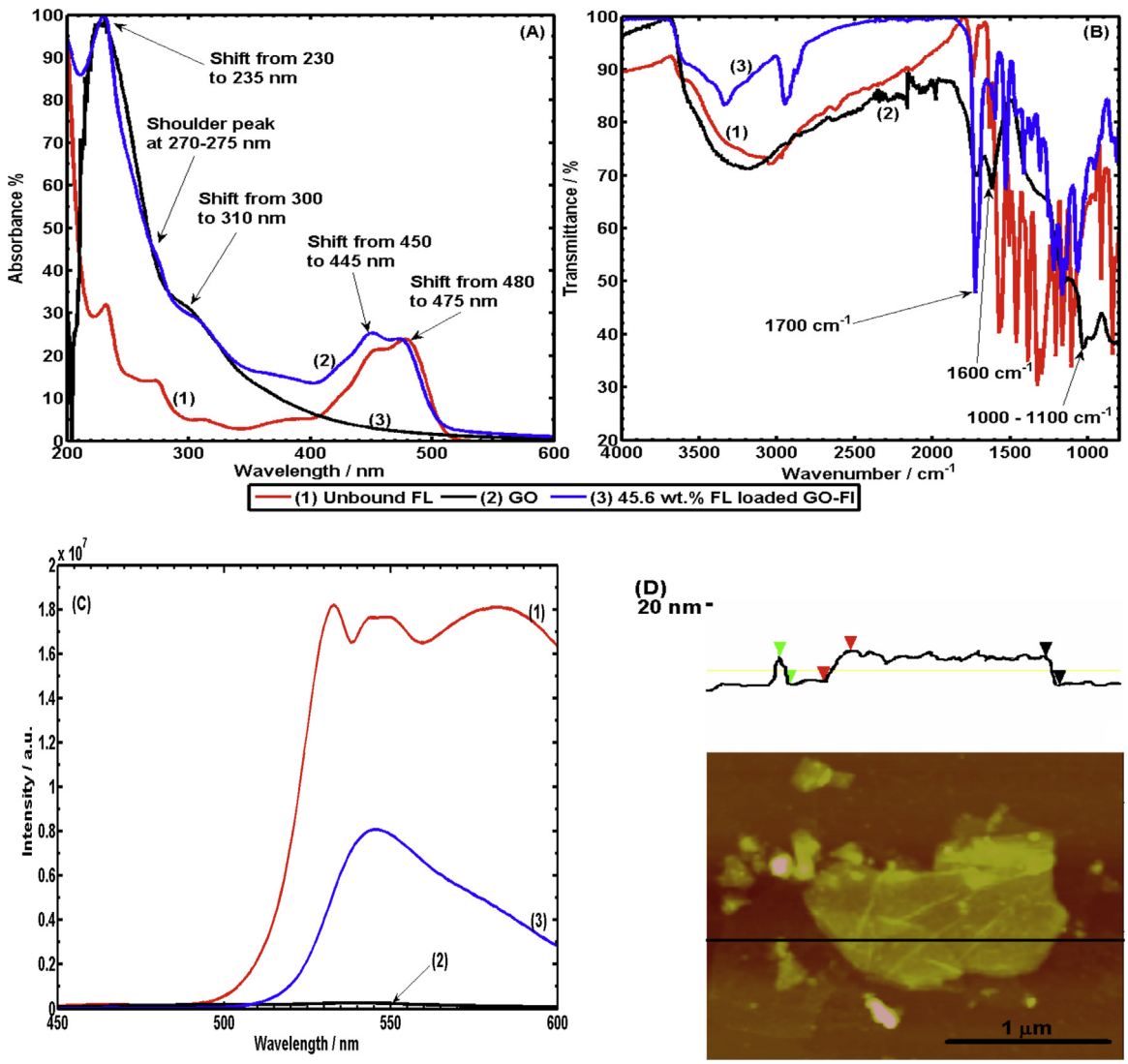

Figure 5. (A) UV-Vis spectra, (B) FT-IR spectra and (C) Photoluminescence spectra of (1) unbound FL, (2) GO and (3) 45.6 wt % loaded GO–FL hybrid. (D) AFM image of a GO–FL sheet from the 45.6 wt % loaded GO–FL solution, showing a sheet of 8.3 nm, 9.4 nm and 8.7 nm thick at the green, red and black arrow points.

previous speculation of drug diffusing away from GO (Sun et al., 2008a,b). The peaks at 450 nm were used to calculate the drug release amounts, and the results are discussed subsequently.

Figure 6 (A) shows the cumulative quantity (%) in a neutral environment (pH = 7.4) over 144 h. There are different release profiles for the samples containing the following loading ratios; FL equal to 21.8 wt %, 45.6 wt % and 58.3 wt % of the GO–FL nanohybrid while the GO content in the nanocomposite is fixed at 2 wt %. The sample containing a 21.8 wt % loading reaches a drug level plateau after 9 h of 66% of the drug in the sample, or 75 μg ml^{-1}. The sample containing a 45.6 wt % loading is slower to reach the plateau, achieving maximum release at 24 h, 62% of the drug in the sample or 2.2 μg ml^{-1}. After 12 h, a 59% release has been achieved, showing the possibility of a rapid but strong drug delivery system of 2 μg ml^{-1} in 12 h. The nanocomposite containing a 58.3 wt % drug loading took 96 h to reach the maximum release level (60% of total available drug or 3.75 μg ml^{-1}). There is a relationship between the degree of drug loading and the time taken to reach the plateau, which can be explained by the drug concentration gradient. Initially, the release medium has 0% drug concentration, and therefore the diffusion from the nanocomposite to the release medium is fast. As the drug concentration in the release medium increases, the diffusion of the drug from the nanocomposite decreases. By varying the loading of the drug onto the GO, the drug release rate can be altered to suit the application (i.e. fast release of anaesthetic for pain relief or sustained release of a therapeutic drug). The 45.6 wt % loading percentage sample was chosen to undergo further analysis in acidic drug release conditions and biodegradation analysis as it offered the optimum combination of strong, efficient and fast delivery of a drug as well as drug loading efficiency.

A hybrid of chitosan and unbound FL was created that contains the same mass of FL as the nanocomposite sample containing a 45.6 wt % loading of FL in GO–FL hybrid (Figure 6 (A)). This sample was used to investigate the improvement that bonding a drug to GO can have on the drug release performance. The sample of free FL encapsulated in chitosan has a plateau after 72 h at 36% of the drug in the sample or 1.2 μg ml^{-1}. The unbound FL was unable to diffuse fully through the polymer film and out into the release medium within the 150 h presumably due to the strong hydrogen bonding between FL and chitosan (Figure S4 [Supplemental Information]), which leads to a shift in the 1539 (N–H) and 1018 cm^{-1} (O–H) peak for pristine chitosan to 1537 and 1019 cm^{-1} for the hybrid of chitosan and FL in the FT-IR spectra. In contrast, the nanocomposite sample containing the same amount of FL has both a quicker and more substantial (62% vs. 36%) delivery of the drug than the sample

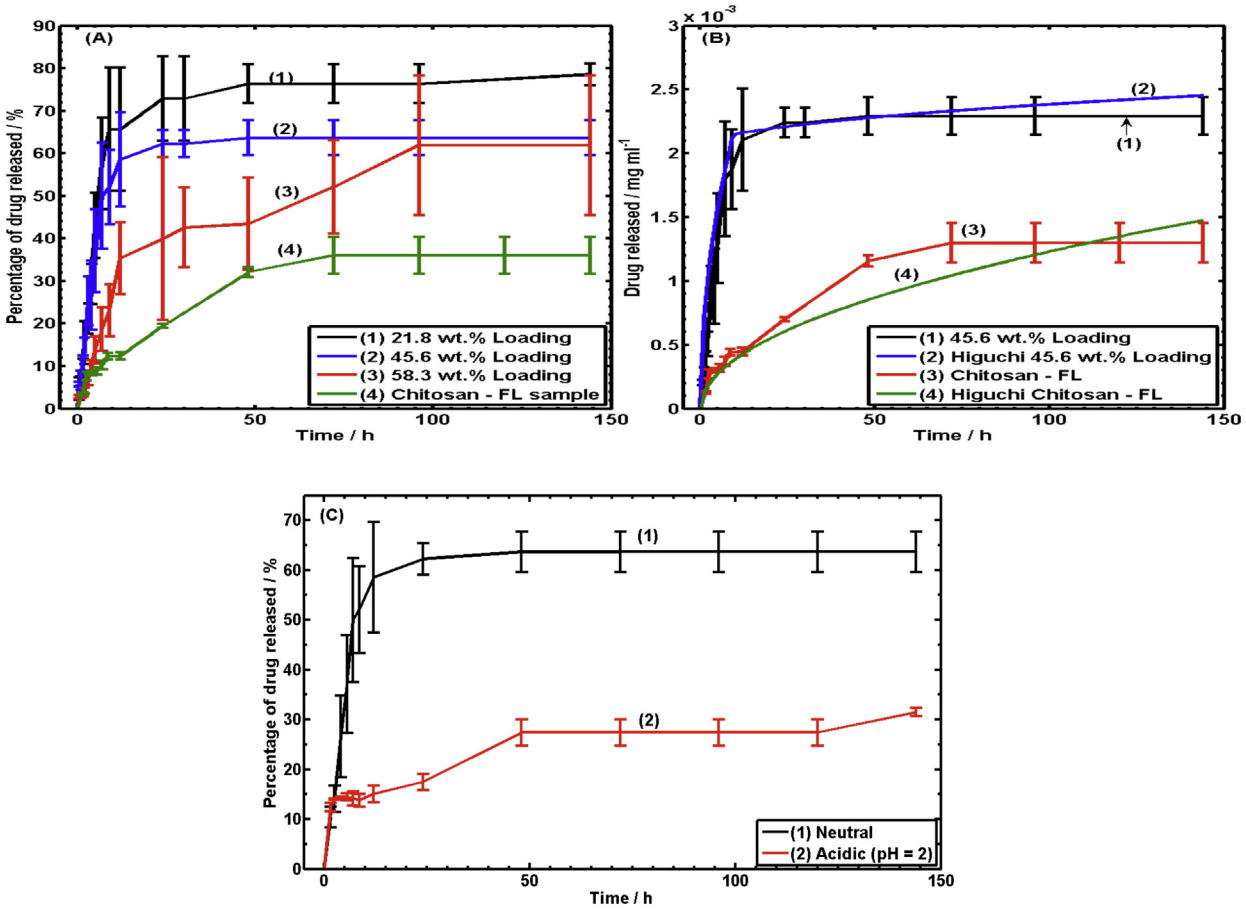

Figure 6. (A) Percentage of drug released from GO–FL nanocomposite (CGO–2%) in comparison to a non-GO Chitosan–FL hybrid in a neutral (pH = 7.4) environment as a function of drug loading. (B) Higuchi equation simulation of drug release from chitosan–FL and chitosan GO–FL nanocomposite. (C) Percentage of drug released from GO–FL nanocomposite in an acidic environment.

of free FL. The hydrophilic GO sheets may have increased the diffusion coefficient of the GO–FL in comparison to unbound FL (see below), raising the speed and the amount of the drug release. Similar to the case in chitosan film, the incomplete release of the drug from the nanocomposite film may be attributed to the strong bonding between GO–FL and chitosan. Figure S4 shows a shift in the 1539 and 1018 cm^{-1} peak for pristine chitosan to 1530 and 1016 cm^{-1} for 58.3 wt % loaded GO–FL in chitosan. This strong bonding restrains the GO–FL hybrid from complete release from the nanocomposite film to the PBS medium.

To further understand the improvement in drug delivery performance that bonding to GO offers, release profiles of drugs in the polymer and nanocomposite were estimated by drug diffusion equations that are commonly used such as the Higuchi equations (Higuchi, 1961; Higuchi, 1963). The standard Higuchi equation defines the cumulative amount of drug released, M_t, as:

$$M_t = k \times \sqrt{t} \tag{3}$$

where t is the time elapsed and k is the Higuchi constant, defined as:

$$k = A x \sqrt{2 \times C_{init} \times D \times C_s} \tag{4}$$

where C_{init} is the initial concentration of the drug within the matrix, A is the cross sectional area of the diffusion matrix, C_s is the drug solubility and D is the drug diffusion coefficient in water, namely 500 mg ml^{-1} and 0.42×10^{-5} cm^2 s^{-1}, respectively for pristine FL (Casalini, Salvalaglio, Perale, Masi, & Cavallotti, 2011). The result of the modelling analysis for the release of unbound FL from chitosan is shown in Figure 6 (B), demonstrating a close correlation to the experimental results and confirming the accuracy of the low release efficiency. However, the Higuchi equation does not model the experimental results for the GO–FL chitosan nanocomposite due to the variations in the drug diffusion coefficient. Using the equation, an approximation of the diffusion coefficient for FL in the nanocomposite can be made, with an initial value of 0.22×10^{-3} cm^2 s^{-1} up to 10 h and then a lower diffusion value of 0.1×10^{-5} cm^2 s^{-1} until the end of the test. The ability to increase the diffusion coefficient could allow for drugs with poor diffusivity in water to be released more efficiently than they would be as an unbound drug. A quicker and more substantial release of these drugs would improve the therapeutic effect of treatments.

GO–FL has been released together from the nanocomposite into the PBS medium, which can be identified by the change of the colour of the PBS (from clear and transparent to a green colour caused by GO–FL, unbound FL turns PBS to yellow), thereby increasing the initial diffusion coefficient of the drug. After having been released into the PBS, FL gradually detached from GO and presented as free FL, as determined from the UV-Vis spectra (Figure S3, Supplemental Information) and discussed previously. This suggests that the free released FL can then diffuse into the cell membranes, leaving the GO to be excreted from the body through the renal system (Yang et al., 2010a,b). The above calculations consider FL as the drug. If GO–FL is considered as a single drug entity, the $C_s \times C_{init}$ will remain the same because the new C_s for GO–FL is 45.6% of the original C_s while the new C_{init} is the 1/45.6% of the original C_{init}, which means the above theoretical values for D will stand. The released GO–FL

complexes could act as nanocarriers for intracellular delivery of the drugs (Rana et al., 2011; Gonçalves et al., 2013).

Figure 6 (C) shows the cumulative percentages of drug released in an acidic environment (pH = 2) from a nanocomposite containing a 45.6 wt % loading of FL in GO–FL hybrid. The nanocomposite placed in acidic conditions released the drug initially in a profile similar to the profile for neutral conditions. A steady release of drug was recorded until a plateau was reached at 144 h (32% of drug within the test samples or 1 $\mu g\ ml^{-1}$). The cumulative quantities of drug released in other acidic environments (pH = 5.5 and 6.5) (Figure S5) are also lower than that in the neutral environment. A reduction in the maximum drug release amount when in an acidic medium offers the possibility of a selective release device with limited release in gastric juices (pH = 1–2) and then a more substantial release when in the neutral media of the intestines (pH = 6–7) or in a targeted disease area where the pH is neutral. In the neutral environment, chitosan swelled in the medium; the presence of the hydrophilic GO facilitated the release of FL as discussed above. In the acidic environment, the hydrophilic GO became hydrophobic and tended to aggregate together, presumably through electrostatic attractions (Bai et al., 2010; Xu, Sheng, Li, & Shi, 2010), thus hindering the release of FL. Furthermore, the solubility of FL may be dramatically decreased as its carboxyl group will be protonated in this case, again hindering the release of FL into the acidic environment. The rapid release of the FL at the beginning of the test may be due to partial dissolution of surface chitosan in the acidic condition, which suppresses the effects of GO aggregation and FL solubility.

The bonding of FL onto GO increases the maximum drug release amount by 72% when compared to unbound FL from a chitosan matrix. The drug release tests show that the drug release behaviour can be altered by varying the drug loading ratio onto the GO. The release profile is sensitive to the pH of the release medium, with the quantity of drug released reduced substantially (by 48%) when in an acidic medium.

3.6. Biodegradation analysis

The effect that GO will have on the biodegradation rate of a polymer has not been analysed in the literature. This can be achieved through a biodegradation test using polymer specific enzymes. Specimens of nanocomposites containing 0 wt % GO (CGO–0%), 2 wt % GO (CGO–2%) and GO–FL with 45.6 wt % FL loading were submerged in a solution of hen egg white lysozyme and PBS to simulate in vivo conditions. Hen egg white lysozyme possesses a similar main chain formation and binding sub-sites as human lysozyme (Nordtveit, Vårum, & Smidsrød, 1996). During the biodegradation analysis, the mass of the samples dropped at different rates (Figure 7). CGO–0% showed the quickest degradation rate of those tested, losing 70 wt % of their initial mass after one week compared to 22 wt % for CGO–2% and 43 wt % for the GO–FL with 45.6 wt % FL loading samples. A change in the colour of the PBS solution containing the GO–FL with 45.6 wt % FL after one week confirmed the release of the drug into the medium containing the enzyme during the biodegradation test. The initial high degradation rate for all the profiles can be attributed to the lysozyme reaction to the abundant chitosan chains containing at least 3 acetyl units (Nordtveit, Vårum, & Smidsrød, 1994; Sashiwa, Saimoto, Shigemasa, Ogawa, & Tokura, 1990). Lysozyme degrades polysaccharides like chitin and chitosan through enzymatic hydrolysis of the β - (1 ? 4) glycosidic linkages through the hexameric sugar ring binding sites of lysozyme (Freier et al., 2005; Nordtveit et al., 1994).

Once the number of suitable sites has been reduced, the rate of degradation slows between week one and week two and then again between week 2 and week 3 for all specimens. CGO–0% reduced to 15 wt % of their original mass after 2 weeks, compared to 67

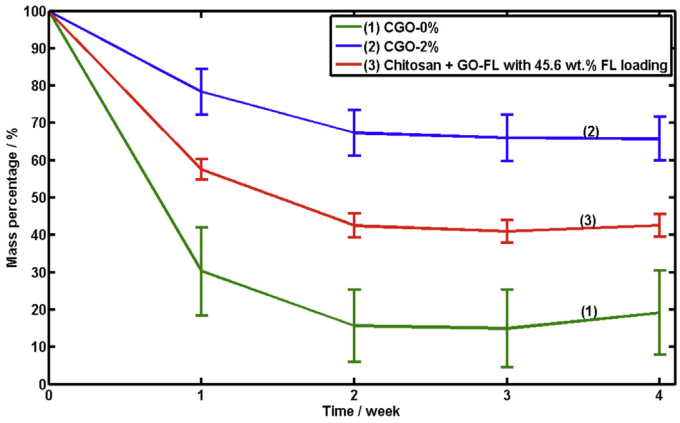

Figure 7. Mass change during enzymatic analysis of nanocomposites containing 0 wt % GO (CGO–0%), 2 wt % GO (CGO–2%), and GO–FL with 45.6 wt % FL loading over 4 weeks.

wt % and 43 wt %, respectively for CGO–2% and the GO–FL with 45.6 wt % FL loading samples. The degradation rate for all samples plateaus around week 2, after which the mass of samples varies no more than 2%. The mass loss curve for pristine chitosan is similar to the previous literature (Freier et al., 2005). The difference in mass loss between the samples can be explained by the presence of the nanoparticles GO and GO–FL. Nanoparticles like graphene and graphene oxide are impermeable to most molecules (Bunch et al., 2008). They may decrease the rate at which the enzymes permeate through a nanocomposite by the tortuous path model that predicts an increase in the barrier properties of nanocomposites (Nielsen, 1967; Sun, Boo, Clearfield, Sue, & Pham, 2008). Furthermore, the adsorption of the chitosan molecular chains onto the GO via strong hydrogen bonding and electrostatic forces can restrict the chain movement, similar to the physical cross-linking effect in polyacrylamide-GO hydrogels (Liu et al., 2012a,b). Cross-linking can act to slow down the cleaving and enzymatic degradation of these macromolecules (Carreño-Gómez & Duncan, 1997), hence the mass loss is lower for the nanocomposites than for the pristine chitosan. The difference in mass loss between CGO–2% and GO–FL with 45.6 wt % FL loading can be attributed to the presence of the drug coating in the latter which limited the bonding sites between GO and chitosan dissolved in the solution.

The effects of GO and GO–FL on the biodegradation of chitosan can also be seen in Figure S6 (Supplemental Information), which shows the surface morphology of the films before the biodegradation test began and 1 week after the test. Among the three samples analyzed, CGO–2% suffered the least pitting and crevassing on the surface during biodegradation, confirming its enhanced resistance to enzymatic activity. In contrast, high aspect ratio extrusions appear in the sample for chitosan–GO–FL (Figure S7, Supplemental Information). These extrusions are chitosan coated GO nanosheets which can be excreted from the body as previously mentioned. GO has been reported to be biocompatible at doses up to 1 mg kg^{-1} of body weight (Zhang et al., 2011a,b). Coating GO with chitosan was shown to further improve the biocompatibility of GO and to limit the cytotoxic effects on cells in *in vitro* tests (Rana et al., 2011). Thus, it is envisaged that these extrusions are non-toxic to the body.

There is no correlation between biodegradation rate and the release rate of the drug as the pristine chitosan film was the fastest to biodegrade over the course of the first week during which it lost more mass (70%) than the nanocomposite of GO–FL, but in the form of a drug eluding polymer it had the slowest release rate and a lower efficiency of delivery with a plateau of delivery after 72 h. The difference between drug delivery performance and biodegradation rate can be explained by the tortuous path that slowed the enzymes

progression into the nanocomposite containing GO–FL and by the chitosan chains that are bound onto the GO surface, making them more difficult to break. The mass loss curve for the sample containing 45.6 wt % FL in GO–FL hybrid over 4 weeks is important to consider when studying drug release from nanocomposites. Over the first week, the nanocomposite lost 43% of its original weight (Figure 7) and released 62% of the available drug (Figure 6 [A]). The nanocomposite will stay intact within the body long enough for a steady and controlled drug delivery to occur before biodegrading and being excreted, as can be seen in SEM analysis after one week (Figures S6 and S7).

4. Conclusions

Biodegradable chitosan nanocomposite films with 0.25 to 5 wt % GO were prepared by solution casting. The nanocomposite containing 2 wt % GO exhibited the best combination of mechanical properties and drug-loading capacity, with the Young's modulus raising from 1 to 1.3 GPa, ultimate tensile strength from 24 to 34 MPa, and elongation at break from 14.5% to 17.7% compared to the pristine chitosan. Improvements of the mechanical properties were attributable to the high stiffness, strength, specific surface area and ample functional groups as well as the mobility of GO sheets under tension.

Drug release tests show that the release profile of the drug from the polymer matrix is dependent on two key factors: the loading ratio of the drug to GO and the pH of the medium that the drug is being released into. In a comparison to chitosan with the same amount of FL, the GO–FL nanohybrid containing 45.6 wt % FL loading released 72% more of the drug and achieved maximum delivery in a shorter time span than the pristine chitosan sample. Different drug release profiles were noted during testing in neutral and acidic media with a reduction of release quantity during the acidic test, showing a pH-sensitive release functionality. Nanocomposites of GO and GO–FL biodegraded slower than pristine chitosan due to the strong bonding of the GO with chitosan and the effect of the tortuous path model on the permeability of the enzyme.

The chitosan–GO nanocomposites with superior mechanical properties and controllable, pH-sensitive drug delivery profiles reported in this work demonstrate high potential in applications as microneedle array materials for transdermal drug delivery.

Acknowledgements

The authors would like to thank the University of Sheffield for a start-up fund and Yinjun Wang and Dawn Bussey for assistance with AFM imaging.

Appendix A. Supplementary data

Supplementary data associated with this article can be found, in the online version, at http://dx.doi.org/10.1016/j.carbpol.2013.12.012.

References

Akbuğa, J., & Durmaz, G. (1994). Preparation and evaluation of cross-linked chitosan microspheres containing furosemide. *International Journal of Pharmaceutics*, *111*(3), 217–222.

Akbuğa, J. (1993). The effect of the physicochemical properties of a drug on its release from chitosonium malate matrix tablets. *International Journal of Pharmaceutics*, *100*(1–3), 257–261.

An, J. E., & Jeong, Y. G. (2013). Structure and electric heating performance of graphene/epoxy composite films. *European Polymer Journal*, *49*(6), 1322–1330.

Bai, H., Li, C., Wang, X., & Shi, G. (2010). A pH-sensitive graphene oxide composite hydrogel. *Chemical Communications*, *46*(14), 2376–2378.

Bal, S. M., Ding, Z., Kersten, G. F. A., Jiskoot, W., & Bouwstra, J. A. (2010). Microneedle-based transcutaneous immunisation in mice with N-trimethyl chitosan adjuvanted diphtheria toxoid formulations. *Pharmaceutical Research*, *27*(9), 1837–1847.

Bal, S. M., Slütter, B., Jiskoot, W., & Bouwstra, J. A. (2011). Small is beautiful: N-trimethyl chitosan-ovalbumin conjugates for microneedle-based transcutaneous immunisation. *Vaccine*, *29*(23), 4025–4032.

Bao, H., Pan, Y., Ping, Y., Sahoo, N. G., Wu, T., Li, L., & Gan, L. H. (2011). Chitosan-functionalized graphene oxide as a nanocarrier for drug and gene delivery. *Small*, *7*(11), 1569–1578.

Bissessur, R., Liu, P. K. Y., White, W., & Scully, S. F. (2006). Encapsulation of polyanilines into graphite oxide. *Langmuir*, *22*(4), 1729–1734.

Brouwer, J., van Leeuwen-Herberts, T., & de Ruit, M. O. (1984). Determination of lysozyme in serum, urine, cerebrospinal fluid and feces by enzyme immunoassay. *Clinica Chimica Acta*, *142*(1), 21–30.

Bunch, J. S., Verbridge, S. S., Alden, J. S., van der Zande, A. M., Parpia, J. M., Craighead, H. G., & McEuen, P. L. (2008). Impermeable atomic membranes from graphene sheets. *Nano Letters*, *8*(8), 2458–2462.

Busilacchi, A., Gigante, A., Mattioli-Belmonte, M., Manzotti, S., & Muzzarelli, R. A. A. (2013). Chitosan stabilizes platelet growth factors and modulates stem cell differentiation toward tissue regeneration. *Carbohydrate Polymers*, *98*(1), 665–676.

Carreño-Gómez, B., & Duncan, R. (1997). Evaluation of the biological properties of soluble chitosan and chitosan microspheres. *Int. J Pharm.*, *148*(2), 231–240.

Casalini, T., Salvalaglio, M., Perale, G., Masi, M., & Cavallotti, C. (2011). Diffusion and aggregation of sodium fluorescein in aqueous solutions. *Journal of Physical Chemistry B*, *115*(44), 12896–12904.

Chaudhry, A. U., & Mittal, V. (2013). High-density polyethylene nanocomposites using masterbatches of chlorinated polyethylene/graphene oxide. *Polymer Engineering and Science*, *53*(1), 78–88.

Chen, B., & Evans, J. R. G. (2006). Nominal and Effective Volume Fractions in Polymer - Clay Nanocomposites. *Macromolecules*, *39*(5), 1790–1796.

Chen, S., Wu, Q., Mishra, C., Kang, J., Zhang, H., Cho, K., & Ruoff, R. S. (2012). Thermal conductivity of isotopically modified graphene. *Nature Materials*, *11*(3), 203–207.

Dasari, A., Yu, Z. Z., & Mai, Y. W. (2007). Transcrystalline Regions in the Vicinity of Nanofillers in Polyamide-6. *Macromolecules*, *40*(1), 123–130.

Fang, M., Wang, K., Lu, H., Yang, Y., & Nutt, S. (2010). Single-layer graphene nanosheets with controlled grafting of polymer chains. *Journal of Materials Chemistry*, *20*(10), 1982–1992.

Feng, L., Zhang, S., & Liu, Z. (2011). Graphene based gene transfection. *Nanoscale*, *3*(3), 1252–1257.

Freier, T., Koh, H. S., Kazazian, K., & Shoichet, M. S. (2005). Controlling cell adhesion and degradation of chitosan films by N-acetylation. *Biomaterials*, *26*(29), 5872–5878.

Galvan-Sanchez, A., Urena-Nunez, F., Flores-Llamas, H., & Lopez-Castanares, R. (1999). Determination of the crystallinity index of iron polymethacrylate. *Journal of Applied Polymer Science*, *74*(4), 995–1002.

Gao, J., Bao, F., Feng, L., Shen, K., Zhu, Q., Wang, D., & Yan, C. (2011). Functionalized graphene oxide modified polysebacic anhydride as drug carrier for levofloxacin controlled release. *RSC Advances*, *1*(9), 1737–1744.

Geim, A. K., & Novoselov, K. S. (2007). The rise of graphene. *Nature Materials*, *6*(3), 183–191.

Gonçalves, M., Figueira, P., Maciel, D., Rodrigues, J., Shi, X., Tomás, H., & Li, Y. (2013). Antitumor Efficacy of Doxorubicin-Loaded Laponite/Alginate Hybrid Hydrogels. Macromolecular Bioscience, unpublished, doi: 10.1002/mabi.201300241.

Guo, Y., Sun, X., Liu, Y., Wang, W., Qiu, H., & Gao, J. (2012). One pot preparation of reduced graphene oxide (RGO) or Au (Ag) nanoparticle-RGO hybrids using chitosan as a reducing and stabilizing agent and their use in methanol electrooxidation. *Carbon*, *50*(7), 2513–2523.

Han, D., Yan, L., Chen, W., & Li, W. (2011). Preparation of chitosan/graphene oxide composite film with enhanced mechanical strength in the wet state. *Carbohydrate Polymers*, *83*(2), 653–658.

Higuchi, T. (1963). Mechanism of sustained-action medication. Theoretical analysis of rate of release of solid drugs dispersed in solid matrices. *Journal of Pharmacological Sciences*, *52*(12), 1145–1149.

Higuchi, T. (1961). Rate of release of medicaments from ointment bases containing drugs in suspension. *Journal of Pharmacological Sciences*, *50*(10), 874–875.

Hou, W. M., Miyazaki, S., Takada, M., & Komai, T. (1985). Sustained release of indomethacin from chitosan granules. *Chemical & Pharmaceutical Bulletin*, *33*(9), 3986–3992.

Jameela, S. R., & Jayakrishnan, A. (1995). Glutaraldehyde cross-linked chitosan microspheres as a long acting biodegradable drug delivery vehicle: studies on the in vitro release of mitoxantrone and in vivo degradation of microspheres in rat muscle. *Biomaterials*, *16*(10), 769–775.

Kim, H., Abdala, A., & Macosko, C. W. (2010). Graphene/polymer nanocomposites. *Macromolecules*, *43*(16), 6515–6530.

Knapczyk, J. (1993). Chitosan hydrogel as a base for semisolid drug forms. *International Journal of Pharmaceutics*, *93*(1-3), 233–237.

Kristl, J., Šmid-Korbar, J., Štruc, E., Schara, M., & Rupprecht, H. (1993). Hydrocolloids and gels of chitosan as drug carriers. *International Journal of Pharmaceutics*, *99*(1), 13–19.

Kumar, M. N. V. R., Muzzarelli, R. A. A., Muzzarelli, C., Sashiwa, H., & Domb, A. J. (2004). Chitosan chemistry and pharmaceutical perspectives. *Chemical Reviews*, *104*(12), 6017–6084.

Layek, R. K., Samanta, S., & Nandi, A. K. (2012). Graphene sulphonic acid/chitosan nano biocomposites with tunable mechanical and conductivity properties. *Polymer*, *53*(11), 2265–2273.

Lee, C., Wei, X., Kysar, J. W., & Hone, J. (2008). Measurement of the elastic properties and intrinsic strength of monolayer graphene. *Science*, *321*(5887), 385–388.

Liu, H. W., Hu, S. H., Chen, Y. W., & Chen, S. Y. (2012). Characterization and drug release behavior of highly responsive chip-like electrically modulated reduced graphene oxide–poly(vinyl alcohol) membranes. *Journal of Materials Chemistry*, *22*(33), 17311–17320.

Liu, R., Liang, S., Tang, X. Z., Yan, D., Li, X., & Yu, Z. Z. (2012). Tough and highly stretchable graphene oxide/polyacrylamide nanocomposite hydrogels. *Journal of Materials Chemistry*, *22*(28), 14160–14167.

Liu, K., Zhang, J. J., Cheng, F. F., Zheng, T. T., Wang, C., & Zhu, J.-J. (2011). Green and facile synthesis of highly biocompatible graphene nanosheets and its application for cellular imaging and drug delivery. *Journal of Materials Chemistry*, *21*(32), 12034–12040.

Liu, Z., Robinson, J. T., Sun, X., Yang, K., & Dai, H. (2009). PEGylated Nano-Graphene Oxide for Delivery of Water Insoluble Cancer Drugs. *Journal of the American Chemical Society*, *130*(33), 10876–10877.

Liu, Z., Robinson, J. T., Tabakman, S. M., Yang, K., & Dai, H. (2011). Carbon materials for drug delivery & cancer therapy. *Materials Today*, *14*(7-8), 316–323.

Lorenzo-Lamosa, M., Remuñán-López, C., Vila-Jato, J., & Alonso, M. (1998). Design of microencapsulated chitosan microspheres for colonic drug delivery. *Journal of Controlled Release*, *52*(1-2), 109–118.

Marcano, D. C., Kosynkin, D., Berlin, V., Sinitskii, J. M., Sun, A., Slesarev, Z., & Tour, A. J. M. (2010). Improved synthesis of graphene oxide. *ACS Nano*, *4*(8), 4806–4814.

Muzzarelli, R. A. A. (2012). Nanochitins and Nanochitosans, Paving the Way to Eco-Friendly and Energy-Saving Exploitation of Marine Resources. In K. Matyjaszewski, & M. Möller (Eds.), *Polymer Science: A Comprehensive Reference* (10) (pp. 153–164). Amsterdam: Elsevier BV.

Muzzarelli, R. A. A., Boudrant, J., Meyer, D., Manno, N., DeMarchis, M., & Paoletti, M. G. (2012). Current views on fungal chitin/chitosan, human chitinases, food preservation, glucans, pectins and inulin: A tribute to Henri Braconnot, precursor of the carbohydrate polymers science, on the chitin bicentennial. *Carbohydrate Polymers*, *87*(2), 995–1012.

Nielsen, L. E. (1967). Models for the Permeability of Filled Polymer Systems, *Journal of Macromolecular Science. Pure and Applied Chemistry*, *1*(5), 929–942.

Nordtveit, R., Vårum, K. M., & Smidsrød, O. (1994). Degradation of fully water-soluble, partially N-acetylated chitosans with lysozyme. *Carbohydrate Polymers*, *23*(4), 253–260.

Nordtveit, R., Vårum, K. M., & Smidsrød, O. (1996). Degradation of partially N-acetylated chitosans with hen egg white and human lysozyme. *Carbohydrate Polymers*, *29*(2), 163–167.

Novoselov, K. S., Geim, A. K., Morozov, S., Jiang, V., Zhang, D., Dubonos, Y., & Firsov, V. S. A. (2004). Electric field effect in atomically thin carbon films. *Science*, *306*(5696), 666–669.

Nunes, C., Mahendrasingam, A., & Suryanarayanan, R. (2005). Quantification of crystallinity in substantially amorphous materials by synchrotron X-ray powder diffractometry. *Pharmaceutical Research*, *22*(11), 1942–1953.

Pan, Y., Bao, H., & Li, L. (2011). Noncovalently functionalized multiwalled carbon nanotubes by chitosan-grafted reduced graphene oxide and their synergistic reinforcing effects in chitosan films. *ACS Applied Materials & Interfaces*, *3*(12), 4819–4830.

Pan, Y., Wu, T., Bao, H., & Li, L. (2011). Green fabrication of chitosan films reinforced with parallel aligned graphene oxide. *Carbohydrate Polymers*, *83*(4), 1908–1915.

Porstmann, B., Jung, K., Schmechta, H., Evers, U., Pergande, M., Porstmann, T., & Krause, H. (1989). Measurement of lysozyme in human body fluids: Comparison of various enzyme immunoassay techniques and their diagnostic application. *Clinical Biochemistry*, *22*(5), 349–355.

Portero, A., Remuñán-López, C., & Vila-Jato, J. (1998). Effect of chitosan and chitosan glutamate enhancing the dissolution properties of the poorly water soluble drug nifedipine. *International Journal of Pharmaceutics*, *175*(1), 75–84.

Rana, V. K., Choi, M. C., Kong, J. Y., Kim, G. Y., Kim, M. J., Kim, S. H., & Ha, C. S. (2011). Synthesis and Drug-Delivery Behavior of Chitosan-Functionalized Graphene Oxide Hybrid Nanosheets. *Macromolecular Materials and Engineering*, *296*(2), 131–140.

Rao, S., & Sharma, C. (1997). Use of chitosan as a biomaterial: studies on its safety and hemostatic potential. *Journal of Biomedical Materials Research*, *34*(1), 21–28.

Sari, M. M. (2013). Fluorescein isothiocyanate conjugated graphene oxide for detection of dopamine. *Materials Chemistry and Physics*, *138*(2), 843–849.

Sashiwa, H., Saimoto, H., Shigemasa, Y., Ogawa, R., & Tokura, S. (1990). Lysozyme susceptibility of partially deacetylated chitin. *International Journal of Biological Macromolecules*, *12*(5), 295–296.

Sawayanagi, Y., Nambu, N., & Nagai, T. (1982). Directly compressed tablets containing chitin or chitosan in addition to lactose or potato starch. *Chemical & Pharmaceutical Bulletin*, *30*(8), 2935–2940.

Stoller, M. D., Park, S., Zhu, Y., An, J., & Ruoff, R. S. (2008). Graphene-based ultracapacitors. *Nano Letters*, *8*(10), 3498–3502.

Suk, J. W., Piner, R. D., An, J., & Ruoff, R. S. (2010). Mechanical properties of monolayer graphene oxide. *ACS Nano*, *4*(11), 6557–6564.

Sun, L., Boo, W.-J., Clearfield, A., Sue, H.-J., & Pham, H. Q. (2008). Barrier properties of model epoxy nanocomposites. *Journal of Membrane Science*, *318*(1-2), 129–136.

Sun, X., Liu, Z., Welsher, K., Robinson, J. T., Goodwin, A., Zaric, S., & Dai, H. (2008). Nano-Graphene Oxide for Cellular Imaging and Drug Delivery. *Nano Research*, *1*(3), 203–212.

Tang, L. C., Wan, Y. J., Yan, D., Pei, Y. B., Zhao, L., Li, Y. B., & Lai, G.-Q. (2013). The effect of graphene dispersion on the mechanical properties of graphene/epoxy composites. *Carbon*, *60*, 16–27.

Tomihata, K., & Ikada, Y. (1997). In vitro and in vivo degradation of films of chitin and its deacetylated derivatives. *Biomaterials*, *18*(7), 567–575.

Tozaki, H., Komoike, J., Tada, C., Maruyama, T., Terabe, A., Suzuki, T., & Muranishi, S. (1997). Chitosan capsules for colon-specific drug delivery: improvement of insulin absorption from the rat colon. *Journal of Pharmacological Sciences*, *86*(9), 1016–1021.

Wang, K., Ruan, J., Song, H., Zhang, J., Wo, Y., Guo, S., & Cui, D. (2010). Biocompatibility of Graphene Oxide. *Nanoscale Research Letters*, *6*(8), 8.

Xie, Y., Xu, B., & Gao, Y. (2005). Controlled transdermal delivery of model drug compounds by MEMS microneedle array. *Nanomedicine*, *1*(2), 184–190.

Xu, Y., Sheng, K., Li, C., & Shi, G. (2010). Self-assembled graphene hydrogel via a one-step hydrothermal process. *ACS Nano*, *4*(7), 4324–4330.

Yang, K., Wan, Ḱ., Zhang, J. Ḱ., Zhang, S., Lee, Y., & Liu, S. Z. (2010). In Vivo Pharmacokinetics, Long-Term Biodistribution, and Toxicology of PEGylated Graphene in Mice. *ACS Nano*, *5*(1), 516–522.

Yang, X., Tu, Y., Li, L., Shang, S., & Tao, X.-M. (2010). Well-dispersed chitosan/graphene oxide nanocomposites. *ACS Applied Materials & Interfaces*, *2*(6), 1707–1713.

Zhang, L., Lu, Z., Zhao, Q., Huang, J., Shen, H., & Zhang, Z. (2011). Enhanced chemotherapy efficacy by sequential delivery of siRNA and anticancer drugs using PEI-grafted graphene oxide. *Small*, *7*(4), 460–464.

Zhang, L., Xia, J., Zhao, Q., Liu, L., & Zhang, Z. (2010). Functional graphene oxide as a nanocarrier for controlled loading and targeted delivery of mixed anticancer drugs. *Small*, *6*(4), 537–544.

Zhang, X., Yin, J., Peng, C., Hu, W., Zhu, Z., Li, W., & Huang, Q. (2011). Distribution and biocompatibility studies of graphene oxide in mice after intravenous administration. *Carbon*, *49*(3), 986–995.